Aerosol Science and Technology
Publication details, including instructions for authors and subscription information:
http://www.tandfonline.com/loi/uast20

An Aerosol-Based Process for Electrostatic Coating of Particle Surfaces with Nanoparticles

Stephanie Sigmund [a], Mingzhou Yu [a b], Jörg Meyer [a] & Gerhard Kasper [a]
[a] Institut für Mechanische Verfahrenstechnik und Mechanik, Karlsruhe Institute of Technology, Karlsruhe, Germany
[b] Institute of Earth Environment, Chinese Academy of Sciences, Xi'an, China
Accepted author version posted online: 12 Nov 2013.Published online: 13 Dec 2013.

To cite this article: Stephanie Sigmund, Mingzhou Yu, Jörg Meyer & Gerhard Kasper (2014) An Aerosol-Based Process for Electrostatic Coating of Particle Surfaces with Nanoparticles, Aerosol Science and Technology, 48:2, 142-149, DOI: 10.1080/02786826.2013.863422

To link to this article: http://dx.doi.org/10.1080/02786826.2013.863422

Aerosol Science and Technology, 48:142–149, 2014

ISSN: 0278-6826 print / 1521-7388 online
DOI: 10.1080/02786826.2013.863422

An Aerosol-Based Process for Electrostatic Coating of Particle Surfaces with Nanoparticles

Stephanie Sigmund, Mingzhou Yu,* Jörg Meyer, and Gerhard Kasper
Institut für Mechanische Verfahrenstechnik und Mechanik, Karlsruhe Institute of Technology, Karlsruhe, Germany

An aerosol-based process for coating the surface of arbitrary "carrier" particles with other types of (smaller) "coating" particles via mutual electrostatic attraction is described. Its practical viability was tested by depositing negatively charged 12-nm palladium particles on 250-nm silica spheres carrying a charge of approximately +40 units each. At respective concentrations of 3 to 8 × 10^6 particles per cm^3 (with a charge fraction of about 25%) and 1 × 10^4 particles per cm^3, the deposition process runs to completion (i.e., to neutralization of the carrier particles) within less than a minute. Comparative estimates show that electrostatically enhanced deposition rates are up to 50 times higher than purely thermal collisions. Transmission electron micrographs show a fairly uniform distribution of coating particles across the surface of the carrier particles. The electrostatic coating kinetics were determined experimentally via the charge loss of the carrier particles and compared also to numerical simulations using Zebel's model for electrostatic enhancement of the collision kernel. Measured rates were generally within 10–15% of the simulations, except for the very early stages of attachment (the first 10 s), where agreement was found to be rather sensitive to the coating particle concentration, possibly due to space charge effects.

1. INTRODUCTION

Coating (or "decorating") larger particles with discontinuous layers of much smaller particles has various technical applications. Of interest are coatings with metallic "nanodots" such as Pt or Pd in the range of a few nm, e.g., for gas sensors, optical applications or the design of catalysts (Kruis et al. 1998). This can be done with great precision in an aerosol process based on atmospheric pressure chemical vapor deposition (CVD) (Heel and Kasper 2005; Binder et al. 2007). However, CVD is "chemical" in nature and thus rather material dependent; it requires suitable precursors, and in some cases chemical functionalization of the carrier particle surface to control deposition or a match of substrate and coating materials. Mechanical processes do not have such constraints. A commonly practiced route to coat supermicron particles mechanically is by mixing them with a nanophase such as fumed silica for an extended period of time, e.g., to improve aerosolization of pharmaceuticals used in pDMI devices for inhalation (Meyer and Zimmermann 2004). The limited precision and low efficiency of this method can become a major constraint for coating materials with a high added value.

Electrostatic coating is another, purely physical route that offers considerable flexibility with regard to the combination of particulate materials. It is based on the electrical attraction between charged particles and an oppositely charged substrate. The technique is well established for powder and paint spraying, where high electrical fields are used to deposit easily dispersible supermicron powders onto macroscopic surfaces. In aerosol science, and especially in nanotechnology, the idea of bringing oppositely charged aerosol particles together by mutual attraction is not at all new (Zebel 1958). Borra et al. (1999) demonstrated the advantages of selective bipolar coagulation between two types of oppositely charged droplets containing different chemicals to initiate chemically induced particle generation. Maisels et al. (2000, 2002) used the technique to generate doublets consisting of two different particle materials. However, to the author's knowledge the concept has not been described before as a means for depositing many particles onto the surface of airborne carrier particles.

The principal goals of the current study were to demonstrate the feasibility of such a coating or "decoration" process, to develop experimental methods for an effective investigation of its kinetics—preferably on line—and to compare the measurements with numerical models for electrically enhanced and/or purely thermal coagulation in a bimodal aerosol. The experiments were performed by mixing a low-concentration aerosol of highly charged monodisperse 250-nm silica spheres with a much higher concentration of much smaller metallic nanoparticles carrying one elementary charge at best.

Received 18 June 2013; accepted 30 September 2013.
*Current address: Institute of Earth Environment, Chinese Academy of Sciences, Xi'an, China.
Address correspondence to Stephanie Sigmund, Institut für Mechanische Verfahrenstechnik und Mechanik, Karlsruhe Institute of Technology, Straße am Forum 8, Karlsruhe 76131, Germany. E-mail: stephanie.sigmund@kit.edu

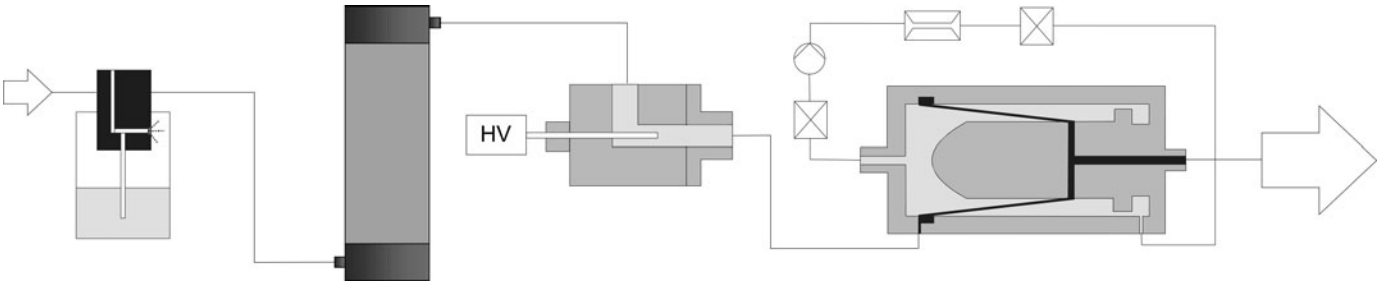

FIG. 1. Setup for generation of a highly charged carrier particle aerosol.

2. EXPERIMENTAL TECHNIQUES

2.1. Generation and Characteristics of an Electrically Charged Carrier Particle Aerosol

The experimental setup used to generate the carrier particle aerosol is shown in Figure 1. An aqueous suspension of monodisperse SiO_2 spheres (1 mg/mL) with diameters of 250 nm $\pm$ 10 nm (Microparticles GmbH) was dispersed into air by a Collison type atomizer (Topas GmbH) and dried in a diffusion dryer. The aerosol was then charged positively in a self-built corona charger to an average of about 40 elementary charges. The resulting charge distribution (Figure 2) was determined from the ratio of the physical particle diameter to the electrical mobility diameter distribution of the spheres obtained by a conventional DMA-CPC technique. In a final mobility classification step, residue particles stemming from nebulization of empty droplets (i.e., drops which do not contain any silica particles but nevertheless generate a small residue particle after evaporation) were removed with a DMA operating at a constant voltage equivalent to a mobility diameter for 250 nm spheres with 40 elementary charges.

The resulting carrier particle size distribution was checked by a conventional SMPS setup (i.e., including particle neutralization). The measurements showed that residue particles had been removed effectively and that the resulting aerosol was indeed monodisperse, consistent with the manufacturer's specifications, except for a minute fraction of doublets as shown in Figure 3. The three main peaks at 250 nm, 165 nm, and 121 nm correspond to 250 nm silica particles in Boltzmann equilibrium carrying one, two, and three elementary charges, respectively. The small peak at 334 nm is most likely due to doublets, which are expected to have a mobility equivalent size about 1.3 times larger than the singlet diameter (Kasper 1983). The fraction of doublets was quite small, however, and rarely visible on transmission electron micrographs. The carrier particle concentration was held constant at a low level 1×10^4 particles per cm^3, in order to avoid electrostatic dispersion.

2.2. Generation and Characterization of the Coating Particle Aerosol

The experimental setup to generate a negatively charged coating particle aerosol is shown in Figure 4. Pd particles were generated by evaporation and condensation in a glowing wire generator (GWG), a technique that has been used repeatedly in aerosol technology and was described recently, e.g., by Peineke et al. (2006). A palladium wire was held at a constant temperature by controlled electrically heating (5.7 V) and a constant gas flow rate of 12.5/min to glow red just below the softening point.

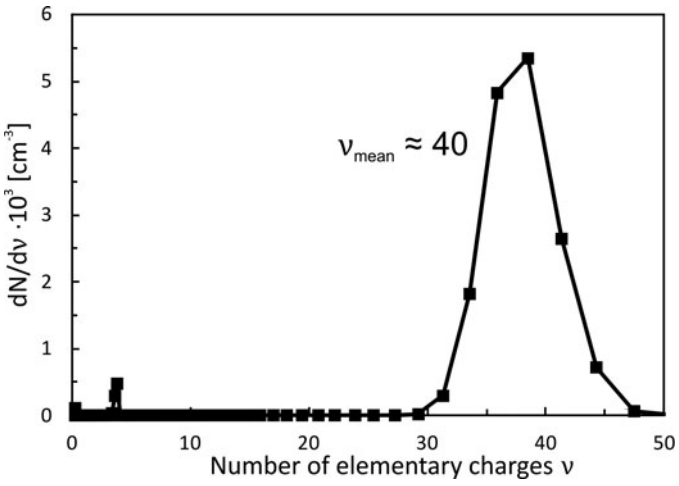

FIG. 2. Carrier particle charge distribution.

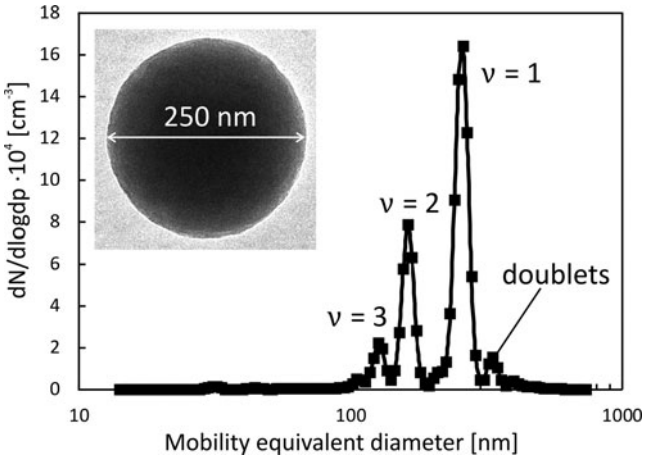

FIG. 3. Mobility size distribution and morphology of uncoated carrier particles in Boltzmann charge state.

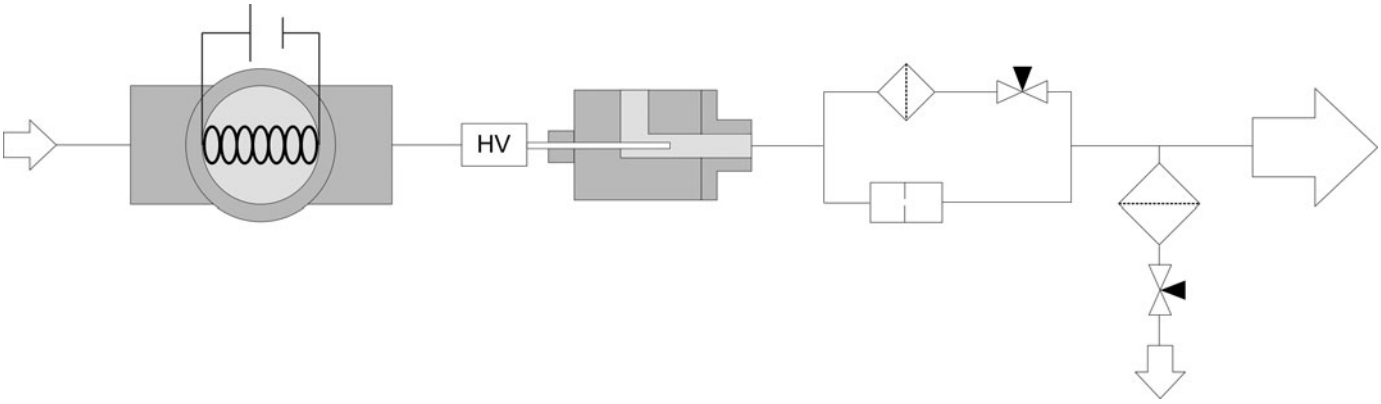

FIG. 4. Setup for generation of charged coating particle aerosol.

(The aerosol concentration was varied downstream of the GWG by dilution.) Throughout all experiments the particle size was thus maintained at a very constant mobility equivalent diameter of 12 nm. As shown in Figure 5, the aerosol consisted of a mix of singlets and small agglomerates formed during the initial generation step. This was, however, an acceptable compromise in order to obtain concentrations of up to about 10^7 particles per cm^3 required for our experiments.

These coating particles were charged negatively in a second corona charger to no more than one elementary charge. Although negative coronas are somewhat more efficient in charging nanoparticles (Alonso et al. 2006) the extrinsic charging efficiency in that set-up was only 25%. This rather modest level was acceptable, however, for the purpose of our investigation into the coating kinetics. A much more efficient method is in the works for larger scale applications. The concentration of the charged Pd aerosol was varied after the charger between 3 and 8 $\times$ 10^6 particles per cm^3 by adjusting the flow through a filtered bypass line as shown in Figure 4. This method does not affect the particle size distribution and the charging. An additional pump allows a reduction of the aerosol volume flow to regulate the mixing ratio between coating to carrier particle aerosol during the subsequent coating step.

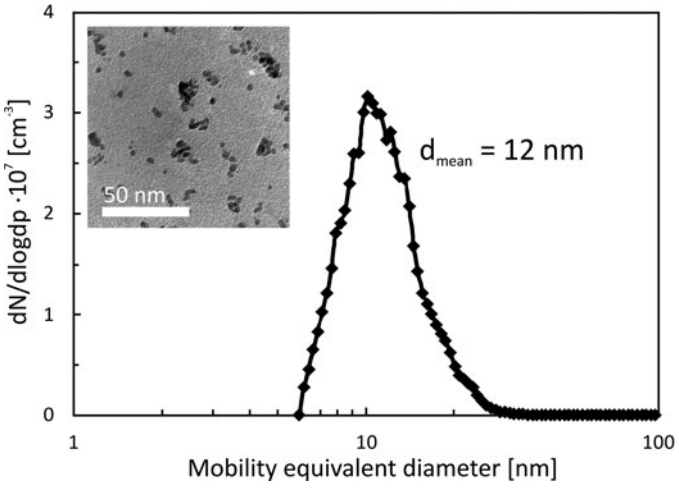

FIG. 5. Morphology and mobility size distribution of the coating particle.

2.3. Coating Process and Measurement of the Coating Rate

The two aerosols were mixed at a volumetric flow ratio of 1:1 by merging them in a y-shaped tube connector. This mixture, consisting of carrier particles with an average of 40 elementary charges and singly or uncharged coating particles, then passed tubes of different length in order to vary residence times and thus coating times τ between 10 and 60 s. The carrier particle concentration was kept constant for all experiments at 1×10^4 particles per cm^3. The coating particle concentration varied from 3 to 8 $\times$ 10^6 particles per cm^3. In other words, there was an excess of coating particles, considering the initial charge and concentration of the carrier particles.

Transmission electron micrographs (TEM) of individual coated carrier particles (Figure 6) were obtained after the maximum residence time of 60 s. Qualitatively the TEM images indicate a significant and fairly uniform surface coverage, as one would expect from electrostatic considerations. They also show that some coating particles on the carrier particle surface were slightly agglomerated, as one would expect from the aerosol size distribution shown in Figure 4. From these images it was not possible to count the number of attached Pd particles with sufficient accuracy for a verification of the coating kinetics, because the silica base material is too dense for the electron beam and thus partly opaque. The TEM images thus only serve as a qualitative illustration of the coating results.

Instead, the attachment rate was determined online via the decrease in net electrical charge of the carrier particles due to their progressive neutralization by oppositely charged coating particles. In essence, one records the shift in peak electrical mobility of the carrier particles with time by a standard DMA+CPC technique, assuming that the change in mobility size of the carrier particles due to gradual attachment of a limited number

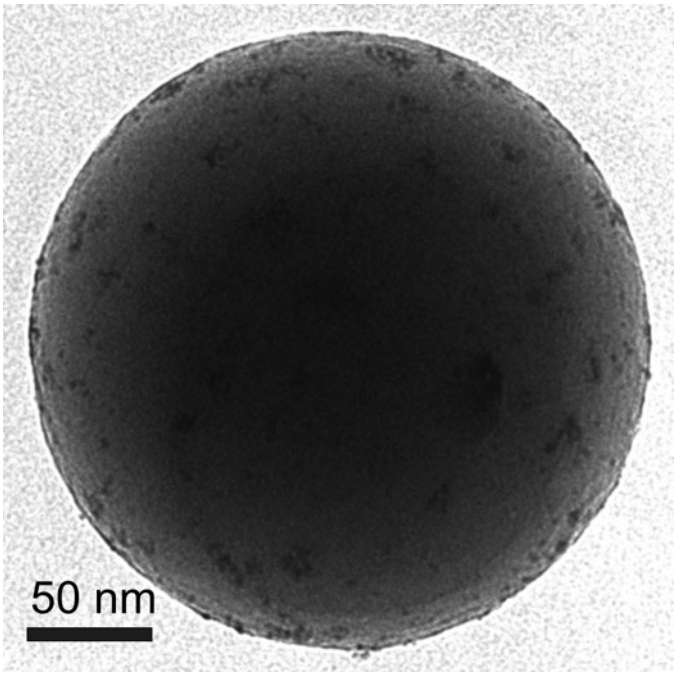

FIG. 6. TEM image of a silica particle with a deposit of Pd particles visible around the edges.

of significantly smaller Pd nanoparticles is negligible. (This assumption was later verified.) Assuming there are no other neutralization effects (see below), the loss of electrical charge corresponds directly to the average number of attached (and previously charged) coating particles per carrier particle. Note that this measurement captures only the electrostatically driven attachment of carrier particles; it is unaffected by any additional attachment due to purely thermal collisions, which was relatively low. (It will be estimated in a subsequent section.)

This mobility-based technique of measuring attachment rates loses accuracy once the majority of carrier particles have been neutralized. The increasing fraction of neutral carrier particles during the final stage of charge-driven attachment was, therefore, determined independently from the difference between total carrier particle concentration and charged carrier particles.

After the charge-driven coating is complete, a few additional coating particles may continue to attach themselves to electrically neutral carrier particles by purely diffusive transport, leading to a slightly negative net charge. This effect was quantified by inverting the polarity of the DMA voltage during the final stage of coating. Diffusion after charging resulted in a final net negative charge level of the aerosol of typically about one or two elementary charges, which is insignificant compared to the charge-driven coating. This secondary effect can be separated easily by simply disregarding the negative part of the charge spectrum.

The possibility of an additional loss of carrier particle charge via ion attachment in a conventional charge neutralization process was also considered. For this purpose the charged carrier particle aerosol was held in the residence time volume for the maximum time of 60 s without adding any coating particles. No change in mean particle charge was detected however.

3. EXPERIMENTAL RESULTS AND DISCUSSION

Measurements of the carrier particle charge distribution were carried out for coating times of 10, 30, and 60 s at coating particle concentrations of 3×10^6, 6×10^6, and 8×10^6 particles per cm^3. The carrier particle concentration was held constant at 1×10^4 particles per cm^3. Figure 7 shows the evolution of the carrier particle cumulative charge distribution for different coating times but otherwise identical conditions. One sees that the coating process has progressed quite far after 1 min even at the lowest concentration of coating particles, but is not yet complete. Some broadening of the carrier particle charge distribution with time is also apparent from the decreasing slope of the curves, presumably caused by a distribution of residence times in the residence time tubes. Such effects can be reduced by further optimization of the system, but this was not the objective of the current study.

Figure 8 shows the influence of the coating particle concentration on the rate of charge loss. The attachment rate is then calculated readily from this graph. Each data point represents an average of typically three measurements. Error bars are not included in the figure, because the variations between measurements were typically on the order of the size of the symbols.

As expected, the agglomeration rate, and thus the attachment rate, is highest during the first 10 s and then slows down due to the decreasing charge difference between carrier and coating particles. The decrease is roughly exponential and accelerates

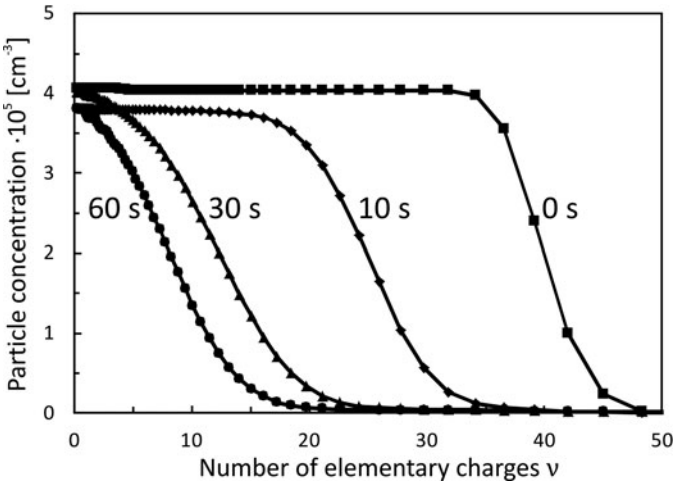

FIG. 7. Evolution of the carrier particle charge as a function of coating time (coating particle concentration 3×10^6 per cm^3). The slight decrease in total concentration indicates the losses of carrier particles during the coating time.

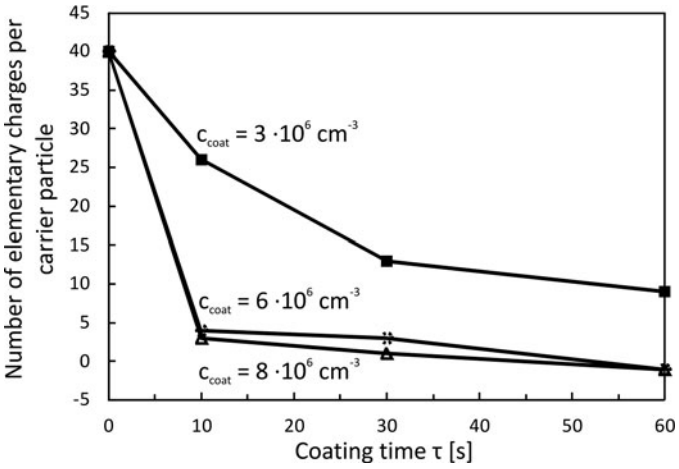

FIG. 8. Mean electrical charge of the carrier particles versus coating time for different coating particle concentrations.

with coating particle concentration. At 8×10^6 particles per cm^3, coating runs nearly to completion within 10 s; within 60 s the carrier particle charge becomes –1 due to diffusive attachment of one additional coating particle. This implies a final coating of 41 Pd particles.

4. NUMERICAL SIMULATION OF THE COATING PROCESS FOR COMPARISON WITH THE EXPERIMENTAL DATA

This section uses numerical simulation to determine the change in net electrical charge of the carrier particles due to attachment of charged coating particles. In Section 4.3 the simulation results are compared directly to the experiments.

Section 4.4 estimates the attachment rate for neutral coating particles on carrier particles due to purely thermal collisions (disregarding any image charge effects due to the initial charge of the carrier particles). Purely thermal collisions represent an additional and independent attachment mechanism, which will be used to estimate the enhancement of the charge-driven coating rates over purely diffusional coating.

4.1. Model Expressions Used

The coagulation rate of a bidispersed aerosol consisting of oppositely charged particles of rather different size was calculated numerically based on well-known population balance models, which have been used many times before to simulate changes in aerosol charge or size distribution (e.g., Eliasson et al. 1991; Park et al. 2005; Verdoold and Marijnissen. 2011). Two coupled balance equations were set up, one for each size fraction. For the coating particles Equation (1) accounts for the change in number density $n(v, q)$ with time as a function of particle volume v and particle charge q:

$$\frac{\partial n(v,q,t)}{\partial t} = \underbrace{\frac{1}{2}\int_0^{q_i}\int_0^{d_i} \beta\left(v', v-v'; q-q', q'\right)}_{\text{self coagulation}} \underbrace{\cdot n\left(v-v', q-q', t\right)\cdot n\left(v', q', t\right) dv'dq' - n(v,q,t)}_{\text{self coagulation}} \underbrace{\cdot \int_0^{\infty}\int_0^{\infty} \beta\left(v, v'; q, q'\right)\cdot n\left(v', q', t\right) dv'dq'}_{\text{self coagulation}} \underbrace{-n(v,q,t)\cdot \int_{-\infty}^{\infty} \beta\left(v, \bar{v}; q, q'\right)\cdot p\left(\bar{v}, q', t\right) dq'}_{\text{bipolar coagulation}} \underbrace{-\frac{\partial n(v,q,t)}{\partial t}}_{\text{diffusion loss}} \underbrace{-\frac{\partial n(v,q,t)}{\partial t}}_{\text{electrostatic dispersion}} \quad [1]$$

The first two terms account for self-coagulation among coating particles. The third term describes bipolar coagulation between coating and carrier particles. This coupling term again assumes that each collision reduces the carrier particle charge by 1. Particle losses due to diffusion and electrostatic dispersion are considered as well.

The population balance for the carrier particles (Equation (2)) neglects self-coagulation among carrier particles, due to their high level of charge. It further assumes that their mean size $\bar{v}$ is not changed by the attachment of coating particles. The carrier particle number density $p(v, q, t)$ can, therefore, only change with time due to bipolar coagulation with coating particles, or by losses to the walls.

$$\frac{\partial p(\bar{v},q,t)}{\partial t} = \underbrace{\int_0^{\infty}\int_q^{\infty} \beta\left(v', \bar{v}; q', q-q'\right)\cdot p\left(\bar{v}, q', t\right)}_{\text{bipolar coagulation}} \underbrace{\cdot n\left(v', q-q', t\right) dq'dv' - p(\bar{v},q,t)\int_0^{\infty}\int_0^{\infty} \beta\left(v', \bar{v}; q, q'\right)}_{\text{bipolar coagulation}} \underbrace{\cdot n\left(v', q', t\right) dq'dv'}_{\text{bipolar coagulation}} \underbrace{-\frac{\partial p(\bar{v},q,t)}{\partial t}}_{\text{diffusion loss}} \underbrace{-\frac{\partial p(\bar{v},q,t)}{\partial t}}_{\text{electrostatic dispersion}} \quad [2]$$

The collision kernel β accounts for the particle charge via a charge correction factor C according to (Zebel 1958):

$$\beta(v, v', q, q') = \beta(v, v', 0, 0)\cdot c_{\text{el}}(q, q'),$$

where

$$c_{\text{el}}(q, q') = \frac{y}{e^y - 1} \quad \text{with} \quad y = \frac{1}{4\pi\varepsilon_0}\frac{qq'e^2}{(v^{1/3} + v'^{1/3})\cdot kT}. \quad [3]$$

The collision frequency for uncharged spheres $\beta(v, v', 0, 0)$ was calculated according to the well-known Model of Fuchs (1964), which requires no further explanation:

$$\beta\left(v, v', 0, 0\right) = 2 \cdot \pi \cdot \left(D + D'\right) \cdot \left(v^{1/3} + v'^{1/3}\right) \cdot \left(\frac{v^{1/3} + v'^{1/3}}{v^{1/3} + v'^{1/3} + 2 \cdot \sqrt{\delta^2 + \delta'^2}} + \frac{8 \cdot \left(D + D'\right)}{\sqrt{\bar{v}^2 + \bar{v}'^2} \cdot \left(v^{1/3} + v'^{1/3}\right)} \right)^{-1} \quad [4]$$

Image potential effects were not included in the calculations.

Diffusion losses were estimated from the equally well-known expressions by Gormley and Kennedy (1949) for the penetration P of particles through a cylindrical duct of length L in laminar flow at flow rate Q and mean flow velocity U:

$$\begin{aligned} P &= 1 - 2.56\Pi^{2/3} + 1.2\Pi + 0.176\Pi^{4/3} \quad (\text{for } \Pi < 0.02) \\ P &= 0.819\exp(-3.66\Pi) + 0.0975\exp(22.3\Pi) \\ &\quad + 0.0325\exp(-57\Pi) \quad (\text{for } \Pi > 0.02)) \\ \Pi &= \frac{\pi DL}{Q} = \frac{\pi DU}{Q} t. \end{aligned} \quad [5]$$

The change of particle concentration caused by deposition in the residence time volume can thus be expressed by

$$\frac{\partial n(v, q, t)}{\partial t} = n(v, q, 0) \cdot \frac{\partial P}{\partial t}. \quad [6]$$

Besides diffusion, particle losses are also caused by repulsive interactions between charges of the same polarity and thus between charged particles. These wall losses due to electrostatic dispersion can be estimated according to the equation (Kasper 1981)

$$\frac{\partial n(v, q, t)}{\partial t} = -4\pi B \cdot q^2 \cdot n(v, q, t)^2 \quad [7]$$

wherein B is the particle mobility.

4.2. Computational Procedures and Validation

All initial values, such as concentrations, particle sizes and charges, were chosen according to experimental conditions. Calculations were thus carried out for coating particle concentrations of 3×10^6, 6×10^6, and 8×10^6 particles per cm^3 at a carrier particle concentration of 10^4 particles per cm^3 and an initial charge state of 40 elementary charges per particle. Carrier particles as well as the coating particles are assumed to be monodisperse initially with respective diameters of 250 nm and 12 nm. The fraction of charged coating particles was assumed to be 25%. (Any effects of the uncharged fraction are discussed later.)

The coupled Equations (1) and (2) were solved with the sectional method for the total number concentrations of coating and carrier particles in each section

$$N_{k,l} = \int_{q_l}^{q_{l+1}} \int_{v_k}^{v_{k+1}} n(v, q, t)\mathrm{d}v \quad \text{and} \quad P_l = \int_{q_l}^{q_{l+1}} p(\bar{v}, q, t)\mathrm{d}q.$$

Using Equation (1) the expression for N transforms into

$$\frac{\mathrm{d}N_{k,l}(t)}{\mathrm{d}t} = \omega_{k,l} - N_{k,l}(t) \sum_{i=1} \beta_{k;\mathrm{lm}} P_m(t) + \frac{\partial \xi}{\partial t} N_{k,l}(0) - 4\pi B \frac{q^2}{4\pi\varepsilon_0} N_{k,l}(t)^2, \quad [8]$$

where

$$\omega_{k,l} = \begin{cases} -N_{k,l} \sum_{i=1} \sum_{m=1} \beta_{k,i;l,m} N_{i,m} & \text{for } k = 1 \text{ or } l = 1 \\ \frac{1}{2} \sum_{\substack{i=1 \\ j=1}} \sum_{\substack{m=1 \\ n=1}} \chi_{ijk;mnl} \beta_{ij;mn} N_{i,m} N_{j,n} & \\ -N_{k,l} \sum_{i=1} \sum_{m=1} \beta_{k,i;l,m} N_{i,m}; & \text{else} \end{cases}.$$

Here

$$\chi_{ijk,mnl} = \begin{cases} \dfrac{v_{k+1} - (v_i + v_j)}{v_{k+1} - v_k} \cdot \dfrac{q_{l+1} - (q_m + q_n)}{q_{l+1} - q_l} & \text{if} \\ v_k \le v_i + v_j \le v_{k+1} \quad q_l \le q_m + q_n \le q_{l+1} & \\ \dfrac{(v_i + v_j) - v_{k-1}}{v_k - v_{k-1}} \cdot \dfrac{(q_m + q_n)}{q_l - q_{l-1}} & \text{if} \\ v_{k-1} \le v_i + v_j \le v_k \quad q_{l-1} \le q_m + q_n \le q_l & \\ 0 & \text{else} \end{cases}.$$

Similarly, Equation (2) becomes

$$\frac{\mathrm{d}P_l(t)}{\mathrm{d}t} = -P_l(t) \sum_{m=1} \sum_{i=1} \delta\beta_{i;l,m} N_{i,m}(t) + \sum_{m=1} \sum_{i=1} \sum_{i=1} \eta_{i;mnl} \beta_{i;m\cdot n} N_{i,m}(t) P_n(t) + \frac{\partial \xi}{\partial t} P_l(0) - 4\pi B \frac{q^2}{4\pi\varepsilon_0} P_l(t)^2 \quad [9]$$

$$\eta_{i;mnl} = \begin{cases} \dfrac{q_{l+1} - (q_m + q_n)}{q_{l+1} - q_l} & \text{if} \quad q_l \le q_m + q_n \le q_{l+1} \\ \dfrac{(q_m + q_n) - q_{l-1}}{q_l - q_{l-1}} & \text{if} \quad q_{l-1} \le q_m + q_n \le q_l \\ 0 & \text{else} \end{cases}$$

$$\delta = \begin{cases} 0 & q_m = 0 \text{ (coating paritcle charge number)} \\ 1 & \text{else} \end{cases}.$$

By equating the calculated change in carrier particle charge state with the surface coating rate, one can compare theoretical and experimental electrostatic coating rates for different particle concentrations.

4.3. Comparison of Simulated and Measured Attachment of Charged Coating Particles

The comparison of attachment rates is shown in Figure 9, where data points represent measurements, while lines represent the calculated values due to bipolar coagulation using the experimental conditions as input parameters. For the lowest concentration of coating particles, model and experimental data points differ by not more than 2 to 3 coating particles, which can be considered good agreement. With increasing concentration, however, our model underestimates the experimental values considerably during the early stage of coating. During this stage coating particle concentrations are still high. We, therefore, suspect that the discrepancy is due to a space charge effect within the cloud of coating particles, which accelerates the coating but is not taken into account by the model. A space charge effect should be proportional to N^2, much like electrostatic dispersion, and therefore be very sensitive to the decline in N with progressing time. (In this context, note again that the comparison is based exclusively on the rate of neutralization of the carrier particles and thus on the attachment of charged coating particles. Neutral species do not enter into model or experiment at this point.)

4.4. Estimate of Purely Thermal Attachment of Uncharged Coating Particles

The purely diffusional attachment of uncharged coating particles represents an additional contribution to carrier particle surface coverage, which can be estimated on the basis of a simplified version of Equation (1), treating diffusive attachment as an independent process:

$$\frac{\partial p(t)}{\partial t} = -\frac{\beta_0}{2} \cdot n \cdot p. \qquad [10]$$

The so calculated coating rate represents an upper limit for purely diffusional attachment because any concentration decrease by self-coagulation and/or diffusional electrostatic losses to the walls is neglected. The coagulation kernel β_0 was calculated from Equation (4). It does not account for any image charge effects caused by the charge level of the carrier particles. Solving the simplified differential Equation (10) leads to the following rate expression:

$$p(t) = \exp\left(-\frac{\beta_0}{2} \cdot n \cdot t\right) \cdot p_0, \qquad [11]$$

wherein p_0 is the starting concentration for the uncharged coating particles at $t = 0$, which is 75% of the total concentration. The results are graphed in Figure 10 for the same three initial concentrations used before. At the highest concentration of coating particles, the maximum attachment by thermal collisions after 60 s is about 5 additional particles over and above the charge-induced coating of 40. At the lowest concentration, it is less than two additional particles. The additional deposition for our range of conditions is thus on the order of about 5 to 10%. Image charge effects are ignored in this estimate.

On the basis of the same absolute concentration, comparison with Figure 9 shows that the charge-induced deposition rate is 7 to 17 times higher than the purely thermal deposition rate when compared for a 60 s coating period, and up to 50 times faster for a 10 s time period.

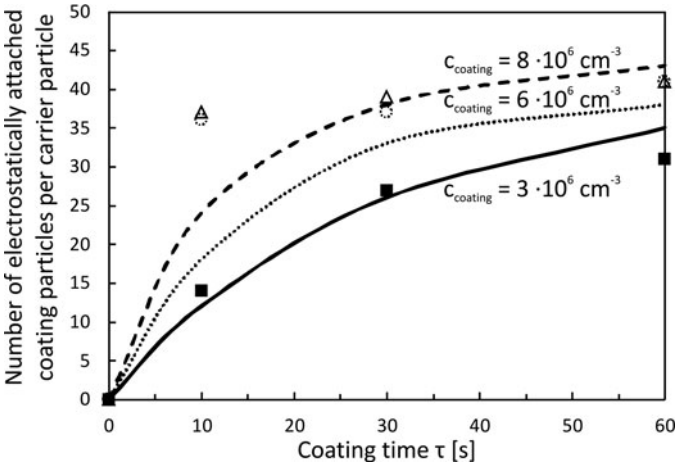

FIG. 9. Comparison of calculated and measured particle attachment versus time for three concentrations of coating particles.

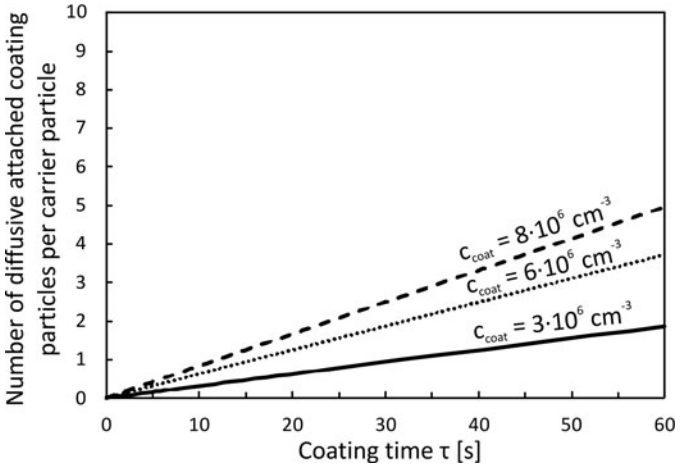

FIG. 10. Attachment of electrically neutral coating particles due to diffusion versus time.

5. SUMMARY AND CONCLUSIONS

A charge-enhanced binary coagulation process has been described to coat an aerosol of 250 nm silica spheres carrying an average charge of 40 e with 12 nm Pd particles carrying at most one elementary charge.

A novel technique was used to measure the electrostatic coating kinetics in real time via the charge loss of the carrier particles by stepwise neutralization due to the attachment of Pd particles.

Coating experiments were performed at various coating particle concentrations in the range of up to 8×10^6 particles per cm^3 (which is roughly 100-fold the carrier particle concentration), and for a range of coagulation times between 10 and 60 s. Under these conditions the electrostatic coating process is shown to be up to 50 times faster than a purely thermal process at comparable concentrations and run to completion in about 60 s or less.

The coagulation process was simulated by numerical solution of coupled population balance equations for carrier and coating particles using Zebel's (1958) model for charge enhancement of the thermal collision frequency. Numerical and experimental results agree to within about ± 3 coating particles per carrier particle, except for the early stages (10 s) of coagulation at higher concentrations of carrier particles, where the simulation underestimates the experimental data substantially. We think this is due to an unaccounted space charge effect among the coating particles.

The objective of this study was to demonstrate the basic feasibility of the coating method and to develop suitable methods of experimental investigation. Obviously there is room for optimization of the process, both with regard to the charging efficiency of the Pd coating particles (which was low), and their efficient use. At the low silica carrier particle concentrations of currently 10^4 particles per cm^3, only about 10% of the Pd is deposited. This can be increased, however, by various means, which will be the objective of another study.

ACKNOWLEDGMENTS

This project is part of the JointLab IP3, a joint initiative of KIT and BASF.

FUNDING

Financial support by the Ministry of Science, Research and the Arts of the State of Baden-Württemberg (Az. 33–729.61–3) is gratefully acknowledged.

REFERENCES

Alonso, M., Martin, M. I., and Alguacil, F. J. (2006). The Measurement of Charging Efficiencies and Losses of Aerosol Nanoparticles in a Corona Charger. *J. Electrostat*., 64:203–214.

Binder, A., Heel, A., and Kasper, G. (2007). Deposition of Palladium Nanodots of Controlled Size and Density onto Surface-Modified SiO_2 Particles by an Atmospheric Pressure CVS/MOCVD Process. *Chem. Vapor Depos*., 13:48.

Borra, J. P., Camelot, D., Chou, K. L., Kooyman, P. J., Marijnissen, J. C. M., and Scarlett, B. (1999). Bipolar Coagulation for Powder Production: Micro-Mixing Inside Droplets. *J. Aerosol Sci*., 30:945–958.

Eliasson, B., and Egli, W. (1991). Bipolar Coagulation Modeling and Applications. *J. Aerosol Sci*., 22:429–440.

Fuchs, N. A. (1964). *The Mechanics of Aerosols*. Pergamon Press, Elmsford, New York.

Gormley, P. G., and Kennedy, M. (1949). Diffusion from a Stream Flowing Through a Cylindrical Tube. *Proc. Royal Irish Acad*., 52(A):163–169.

Heel, A., and Kasper, G. (2005). Production and Characterization of Pd/SiO_2 Catalyst Nanoparticles from a Continuous MOCVS/MOCVD Aerosol Process at Atmospheric Pressure. *Aerosol Sci. Technol*., 39:1027–1037.

Kasper, G. (1981). Electrostatic Dispersion of Homopolar Charged Aerosols. *J. Colloid Interface Sci*., 81:32–40.

Kasper, G. (1983). Note on the Slip Coefficient of Doublets of Spheres. *J. Aerosol Sci*., 14:753–754.

Kruis, F. E., Fissan, H., and Peled, A. (1998). Synthesis of Nanoparticles in the Gas Phase for Electronic, Optical and Magnetic Applications—A Review. *J. Aerosol Sci*., 29:511–535.

Maisels, A., Kruis, F. E., and Fissan, H. (2002). Mixing Selectivity in Bicomponent, Bipolar Aggregation. *J. Aerosol Sci*., 33:35–49.

Maisels, A., Kruis, F. E., Fissan, H., Rellinghaus, B., and Zahres, H. (2000). Synthesis of Tailored Composite Nanoparticles in the Gas Phase. *Appl. Phys. Lett*., 77:4431–4433.

Meyer, K., and Zimmermann, I. (2004). Effect of Glidants in Binary Powder Mixtures. *Powder Technol.,* 139:40–45.

Park, S. H., Lee, K. W., Shimada, M., and Okuyama, K. (2005). Coagulation of Bipolarly Charged Ultrafine Aerosol Particles. *J. Aerosol Sci*., 36, 830–845.

Peineke, C., Attoui, M. B., and Schmidt-Ott, A. (2006). Using Glowing Wire Generator for Production of Charged, Uniformly Sized Nanoparticles at High Concentrations. *J. Aerosol Sci*., 37:1651–1661.

Verdoold, S., and Marijnissen, J. C. M. (2011). Modeling a Bipolar-Coagulation Reactor Using Coupled Population Balances. *J. Electrostat*., 69:240–254.

Zebel, G. (1958). Zur Theorie des Verhaltens elektrisch geladener Aerosole. *Kolloid Zeitschrift*, 157:35–50.